Available online at www.sciencedirect.com
ScienceDirect
Trans. Nonferrous Met. Soc. China 31(2021) 1276−1290
Transactions of Nonferrous Metals Society of China
www.tnmsc.cn

Comparison of castability, mechanical, and corrosion properties of Mg−Zn−Y−Zr alloys containing LPSO and *W* phases

V. E. BAZHENOV, S. S. SAIDOV, Yu. V. TSELOVALNIK, O. O. VOROPAEVA, I. V. PLISETSKAYA, A. A. TOKAR, A. I. BAZLOV, V. A. BAUTIN, A. A. KOMISSAROV, A. V. KOLTYGIN, V. D. BELOV

National University of Science and Technology (MISiS), Leninskiy pr. 4, Moscow, 119049, Russia

Received 21 May 2020; accepted 18 December 2020

Abstract: The Mg–Zn–Y–Zr alloys with long-period stacking-ordered (LPSO) and *W* eutectic phases were investigated to develop new magnesium casting alloys. The temperatures for T6 heat treatment were selected based on the hardness and electrical conductivity measurements. The hot tearing susceptibility of the alloys with LPSO phase is lower than that of the alloys with *W* phase, which is associated with the freezing range of the alloys. However, the investigated alloys displayed the same fluidity. Under T6 conditions, increasing the Y content in the alloys resulted in increased yield strength, whereas other tensile properties were similar for the alloys. The corrosion resistance was higher for the alloys with LPSO phase compared to that of the alloys with *W* phase. Mg−2.5Zn−3.7Y−0.3Zr (mass fraction, %) alloy with LPSO phase possessed high castability and mechanical properties, with a corrosion rate of 2 mm/year.
Key words: magnesium alloy; casting; LPSO phase; *W* phase; fluidity; hot tearing susceptibility; corrosion rate

1 Introduction

Magnesium alloys are commonly used as structure materials in the aircraft and aerospace industries because of their low density and high specific strength. Recently, the applications of magnesium alloys have been extended to include the automobile, electronic, and other industries; hence, there is increased demand for new low-cost and high-performance casting alloys. In the past decades, considerable attention has been focused on the deformation behavior of Mg−Zn−Y alloys [1−4]. However, the Mg−Zn−Y system is an excellent candidate for the development of new magnesium casting alloys.

In the Mg−Zn−Y system, there exist the long-period stacking-ordered (LPSO) phase ($Mg_{12}ZnY$ or $Mg_{21}Zn_2Y_2$) with a variety of structural polytypes, the *W* phase ($Mg_3Zn_3Y_2$ or $MgYZn_2$) with a partially ordered fcc structure, and the *I* phase (Mg_3Zn_6Y) with an ordered icosahedral structure [5−7]. The phases in this system can be arranged in order of decreasing strength as follows: LPSO, *I*, and *W* [5,8−11].

No information has been reported on the fluidity of the Mg–Zn–Y alloys, but the hot tearing behavior of the alloys was investigated. The hot tearing susceptibility is reduced as the quantity of the LPSO phase in alloy structure increases, because of the grain refinement and pinning effect of the LPSO phase on the grain boundaries [12–14]. JIA et al [15] investigated the hot tearing susceptibility of alloys with *W*, *W*+*I*, and *I* phases in their structures. The lowest hot tearing susceptibility was observed for the alloy with the *W* phase because of the less freezing range (130 and 200 °C for the alloys with *W* and *I* phases, respectively). The long freezing range in the alloys with *I* phase promotes the formation of shrinkage porosity; hence, these alloys are not suitable for use as casting alloys [8,16].

Corresponding author: V. E. BAZHENOV, E-mail: V. E. Bagenov@gmail.com
DOI: 10.1016/S1003-6326(21)65577-2

Ignition problems are associated with the melting and heat treatment of magnesium alloys; however, the oxide film with *Y* contributes to the enhanced protective properties and a higher alloy ignition temperature [17]. The influence of various additions such as Zr, Cu, Mn, Ca, Gd, and B on the microstructure and mechanical properties of Mg−Zn−Y alloys was investigated [18−21]. Zr is of great interest because of its significant effect on grain refinement, which contributes to high alloy casting properties [22].

The T4 and T6 heat treatments can be applied to the Mg−Zn−Y alloys. The heat treatment for alloys with high Y and low Zn contents and LPSO phase as the secondary phase promotes high ultimate tensile strengths (UTSs) [23]. Higher yield strength (YS) and elongation (EL) are observed for the alloys with high Zn and low Y contents and with the *I* phase in alloy structure [24]. The alloys with almost equal Zn and Y contents and secondary *W* phase possess intermediate properties [25].

The corrosion behavior of Mg−Zn−Y alloys was investigated previously; however, it has primarily been studied for alloys in as-cast condition or after deformation processing [4,26,27]. During corrosion, the LPSO, *W*, and *I* phases act as the cathodes with respect to *α*-Mg [28,29]. An increase in the amount of the LPSO phase in the alloy leads to an increase in the corrosion rate [4,26,29]. The corrosion resistance of alloys with *I* phase is greater than that of alloys with *I*+*W* and *W* phases in the structure [27].

The aim of this research was to investigate the microstructure of the Mg−Zn−Y−Zr alloys, the phase composition, heat treatment response, fluidity, hot tearing susceptibility, mechanical properties, and corrosion properties to develop a superior prospective casting magnesium alloy.

2 Experimental

As shown in Table 1, five Mg−Zn−Y−Zr alloys were prepared. The difference between the investigated alloys is in the type of eutectic phase that is formed during solidification (LPSO or *W*) and the amount of the eutectic phase. Mg (99.9 wt.% purity), Zn (99.98 wt.%) metals, Mg−20wt.%Y, and Mg−15wt.%Zr and master alloys were used as raw materials. Melting was performed in a steel crucible using a resistance furnace. In order to protect the melt from ignition, an Ar+2vol.%SF_6 gas mixture was used. After the melt was prepared, it was purged with Ar at 760 °C for 3 min and held for 10 min before pouring. The pouring temperature was 760 °C.

The solidus surface projection, phase composition, and alloy solidification pathways were calculated using Thermo-Calc software [30] with version 4 of the TCMG4 magnesium-based alloy database [31].

Table 1 Chemical compositions of alloys

Alloy	Content/wt.%			
	Mg	Zn	Y	Zr
MgZn2.5Y3.5	Bal.	2.51	3.67	0.32
MgZn3.5Y5.5	Bal.	3.71	5.44	0.50
MgZn5.5Y2	Bal.	5.63	2.07	0.54
MgZn5.5Y3.5	Bal.	5.60	3.33	0.65
MgZn5.5Y4.5	Bal.	5.46	4.67	0.70

The fluidity test with the 8 mm U-type channel in the steel mold was used (Fig. 1(a)) for the fluidity measurements and reported as the probe length (mm). The hot tearing susceptibility was determined using the "dog-bone" test shown in Fig. 1(b). Hot tearing susceptibility was measured as the maximum length of the dog-bone section without hot cracks; the fluidity and hot tearing tests were repeated twice for each alloy composition.

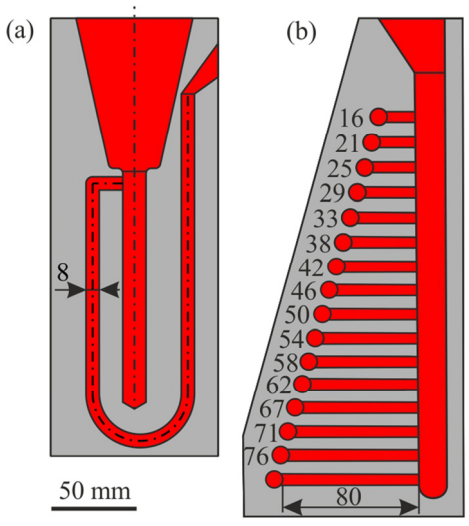

Fig. 1 Diagram of apparatus for U-type fluidity test (a) and "dog-bone" hot tearing test (b) (unit: mm)

The samples for the tensile and corrosion tests were prepared by casting the ingots (340 mm × 50 mm × 32 mm) into a graphite mold and using the T6 heat treatment regime. Cylindrical samples (diameter of 5 mm, and length of 60 mm) were lathe machined and tensile tests were performed using the Instron 5569 universal testing machine.

In order to investigate the heat treatment regimes, rectangular ingots (20 mm × 150 mm × 270 mm) were cast into graphite molds. These ingots were cut into bars (20 mm × 150 mm × 20 mm). One of the bar surfaces was ground for the hardness and electrical conductivity measurements. The Brinell hardness was determined using an Innovatest Nemesis 9001 universal hardness tester. The ball (diameter of 2.5 mm) was held under a load of 613 N for 10 s. The electrical conductivity of the alloys was measured using a contact-free eddy current conductivity meter VE-27NC "Sigma" with a measurement range of 5.0−37.0 MS/m. The heat treatment was performed based on the T6 heat-treatment mode, consisting of a solid solution heat treatment at 540 or 500 °C for 6−18 h followed by quenching in hot water. The quenched samples were aged at 150−300 °C for 4−24 h.

The microstructure of the alloys and content of the elements in the phases were investigated using a Tescan Vega SBH3 scanning electron microscope (SEM) equipped with an Oxford Instruments AZtecEnergy energy-dispersive X-ray spectroscopy (EDS) system. The chemical compositions of the prepared alloys were determined using EDS. Three areas with dimensions of 1 mm × 1 mm were analyzed for each alloy. The volume fractions of phases were estimated using an SEM software by determining the amount of area occupied by each phase in the SEM image. An optical microscope (Carl Zeiss Axio Observer D1m) was used for the microstructural analysis and for calculating grain size. An etchant composed of picric acid (11 g), acetic acid (11 mL), and ethanol (100 mL) was used to reveal the grain boundaries. The grain size was calculated using the linear intercept method.

Alloy phase compositions in the as-cast and heat-treated states were examined using the bulk cylindrical specimens via X-ray diffractometry (XRD) with a Bruker D8 ADVANCE diffractometer under monochromatic Cu K_α radiation.

In order to investigate the corrosion behavior of the alloys, the electrochemical investigations were performed in 3 wt.% NaCl aqueous solution at 25 °C using the IPC Pro MF potentiostat/galvanostat/FRA with the three-electrode corrosion system. The alloy samples served as working electrodes with an exposed area of 1 cm^2. Platinum and saturated silver/silver chloride (Ag/AgCl) electrodes were used as the counter and reference electrodes, respectively. Prior to the electrochemical analysis, the alloy samples were immersed in a 0.3 wt.% HNO_3 aqueous solution for 2 s, which was followed by rinsing in distilled water. Potentiodynamic polarization experiments were performed from the cathodic region (at −2.3 V) to the anodic region (at −1 V) with a scan rate of 1 mV/s. The corrosion current density and corrosion potential were determined from Tafel fitting, and the corrosion rate was calculated [32].

Immersion corrosion tests were performed using rectangular specimens (25 mm × 15 mm × 15 mm) with a surface area of 20 cm^2. The specimens were weighed prior to the tests. Subsequently, the corrosion tests were performed by immersing the samples in the corrosion media for 7 d. Once each test was finished, the sample was extracted and dried. The corrosion products were removed by dipping samples in 200 g/L CrO_3 water solution heated to 80 °C, then neutralized by dipping in 1 mol/L $FeSO_4$ solution for 1 s, and washed with distilled water. The specimens were then re-weighed to determine the mass gain per unit surface area. Finally, the mass loss and corrosion rate (in mm/year) were calculated [33].

3 Results and discussion

3.1 Phase composition calculations

Zr was excluded from further calculations because it did not strongly influence the phase compositions of the analyzed alloys and only impacted the initial temperature of the primary α-Zr phase solidification and the quantity of this phase. Figure 2 shows the Mg-rich corner of Mg−Zn−Y system solidus surface projection calculated via Thermo-Calc software. Depending on the alloy composition, the solidification can end with the formation of either LPSO, *W*, or *I* phases by eutectic/peritectic transitions. Under actual casting conditions, the peritectic transformations would not easily occur; therefore, further discussion would focus on the eutectic transition. The amount of

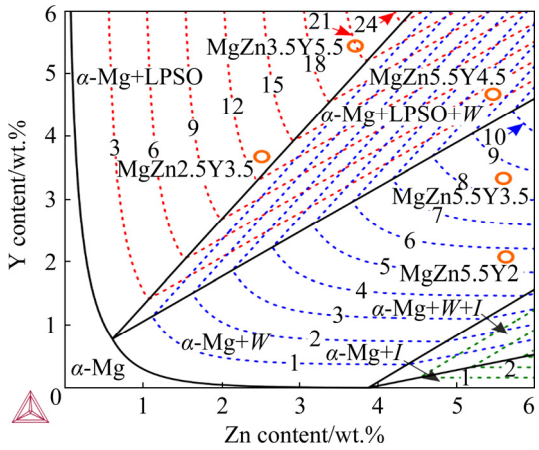

Fig. 2 Calculated solidus surface projection of Mg–Zn–Y system at Mg-rich corner, phase composition plot, and position of prepared alloys (Numbers on red isoline show the amount of LPSO phase; on blue isoline of *W* phase, and on green isoline of *I* phase in wt.%)

eutectic is important for casting alloys because large proportions of eutectics are responsible for the high fluidity and low hot tearing susceptibility of alloys [34]. The amounts (wt.%) of LPSO (red), *W* (blue), and *I* (green) phases are shown in Fig. 2. From the calculations, the amount of Mg in the secondary phase is related to the amount of this phase in the alloy. For example, the LPSO phase ($Mg_{12}ZnY$) is rich in magnesium; hence, its content in the investigated composition area in the phase diagram can be as much as 24 wt.%. Conversely, the quantity of the *I* phase (Mg_3Zn_6Y) with low Mg and high Zn contents is less than 3 wt.%. The *W* ($MgYZn_2$) phase falls in an intermediate position between the aforementioned phases and its content in the eutectic can be up to 11 wt.%. Based on the Thermo-Calc analysis, MgZn2.5Y3.5 and MgZn3.5Y5.5 alloys were chosen, for which solidification results in the formation of 13 and 21 wt.% of the LPSO phase, respectively. Further, MgZn5.5Y2 and MgZn5.5Y3.5 alloys with 6 and 8.5 wt.% of *W* phase, respectively, were selected along with the MgZn5.5Y4.5 alloy consisting of 4.5 and 8 wt.% of the LPSO and *W* phases, respectively.

In actual casting processes, the solidification conditions are far from equilibrium. The solidification pathways of the Mg−Zn−Y alloys that were calculated using the Lever rule (equilibrium solidification) and the Scheil−Gulliver model (non-equilibrium solidification) are shown in Fig. 3 [35]. Figure 3(a) shows that for MgZn2.5Y3.5, MgZn3.5Y5.5, and MgZn5.5Y4.5, the calculated solidification pathways are similar. All the alloys possess nearly the same liquidus temperature (~630 °C). After primary *α*-Mg solidification in the MgZn2.5Y3.5 and MgZn3.5Y5.5 alloys the *α*-Mg+LPSO binary eutectic solidified in the range of 586−575 °C. In the MgZn5.5Y4.5 alloy, the *α*-Mg+*W* binary eutectic solidified but its quantity was very low and the solidification in that alloy ended with *α*-Mg+LPSO+*W* eutectic formation at constant temperature (575 °C). Hence, solidification of the mentioned alloys initiated and ended at the same temperature and had the same very short freezing range of 55 °C under both equilibrium and non-equilibrium conditions. The thermal analyses of alloys with compositions close to those of the investigated alloys show that the LPSO phase is formed at 530−545 °C and the *W* phase is formed at 510−530 °C [12,14]. This means that the actual freezing range can be higher than that calculated by the Thermo-Calc software and must be ~100 °C.

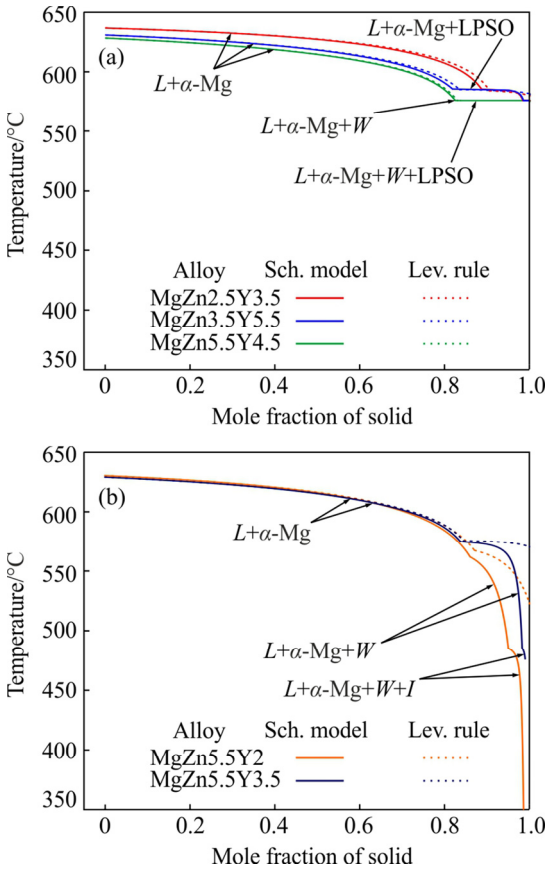

Fig. 3 Equilibrium and non-equilibrium solidification pathways of Mg−Zn−Y alloys calculated via Lever rule and Scheil−Gulliver models, respectively

The solidification pathways of the MgZn5.5Y2 and MgZn5.5Y3.5 alloys are rather different under equilibrium (Lever rule) and non-equilibrium (Scheil−Gulliver) solidification conditions (Fig. 3(b)). Under equilibrium conditions, after the solidification of primary α-Mg, the α-Mg+*W* binary eutectic is solidified in the temperature ranges of 562−522 °C and 575−570 °C for the MgZn5.5Y2 and MgZn5.5Y3.5 alloys, respectively. This means that the equilibrium freezing range is <110 °C for those alloys. Based on the Scheil−Gulliver solidification model in the MgZn5.5Y2 alloy, the α-Mg+*W* binary eutectic is solidified in the temperature range of 562−485 °C, but solidification is not complete. Also, the α-Mg+*W*+*I* ternary eutectic is solidified in the temperature range of 485−341 °C. The same solidification pathway is observed during the non-equilibrium solidification of the MgZn5.5Y3.5 alloy, but with a higher solidus temperature (476 °C). In accordance with the Scheil−Gulliver model, the freezing ranges of the MgZn5.5Y2 and MgZn5.5Y3.5 alloys should be 289 and 154 °C, respectively. The obtained phase transition temperatures also deviate from the experimental results, particularly for the MgZn5.5Y2 alloy. The experimentally obtained freezing range for the MgZn5.2Y0.7 alloy with *I* phase in the structure was 200 °C [9]. Also, the temperature of *I* phase formation was 447 °C in previous research [14]. The solidus temperature (343 °C) can only be obtained in alloys with high Zn content and the Mg_7Zn_3 eutectic phase in the structure [36]. Overall, the freezing ranges for MgZn5.5Y2 and MgZn5.5Y3.5 alloys must be up to 200 °C, which is two times higher than that of alloys with LPSO phases.

3.2 Microstructures

The microstructures of the Mg−Zn−Y−Zr alloys in the as-cast condition and after 6 h of solid solution heat treatment (SSHT) at different temperatures are presented in Fig. 4. In the as-cast microstructure of the MgZn2.5Y3.5 and MgZn3.5Y5.5 alloys, α-Mg is enveloped in light gray and white eutectic phases. Based on the EDS analysis results presented in Table 2, the Zn/Y molar ratios are 0.75:1 and 1.5:1 for the light gray and white phases, respectively. Thus, the light gray phase is LPSO and the white phase is *W*. Contrary to the calculated results presented in Section 3.1, in the MgZn2.5Y3.5 and MgZn3.5Y5.5 alloys, a low quantity of *W* phase is observed. The eutectic with LPSO phase is divorced, but the eutectic with *W* phase is near lamellar with 350 nm spaces between the lamellas. The phase composition of the alloys with 5.5 wt.% Zn and (2−4.5) wt.% Y consists of the primary dendrites of α-Mg and α-Mg+*W* eutectic. No LPSO phase is observed in the MgZn5.5Y4.5 alloy, which does not correlate with the Thermo-Calc calculations. The Zn/Y molar ratios for MgZn5.5Y2, MgZn5.5Y3.5, and MgZn5.5Y4.5 alloys were 1.8:1, 1.7:1, and 1.5:1, respectively. Hence, it is observed that the Y content in the *W* phase is increased with an increase in the Y content of the alloy. As expected, the *W* phase content is also increased with an increase in the Y content of the alloy. Contrary to our results, XU et al [11] reported that XRD results revealed the presence of the *I* phase in the MgZn5.5Y2 alloy. The EDS analysis of MgZn5.5Y2 showed that the Zn/Y molar ratio in some points was ~3:1, which corresponds to the *I* phase; moreover, there is the possibility that both *W* and *I* phases are present in the alloy, which is in accordance with the Scheil−Gulliver solidification calculations. Due to the discrepancy between the Thermo-Calc calculation results and the obtained phase compositions of the alloys, the phase composition of the Mg−Zn−Y and Mg−Zn−Y−Zr alloys in the literature was analyzed and the solidus projection is reconstructed. The reconstructed solidus surface projection is shown in Fig. 5 [1,12,15,25−29, 37−41].

It can be seen that after SSHT at 500 °C for 6 h, the morphologies of the *W* phase in MgZn5.5Y2, MgZn5.5Y3.5, and MgZn5.5Y4.5 alloys changed from lamellar to near globular. Nevertheless, no changes in the *W* or LPSO phase eutectic morphology are observed for the MgZn2.5Y3.5 and MgZn3.5Y5.5 alloys after SSHT at 540 °C for 6 h. The *I* phase transformed into the *W* phase during deformation processing or heat treatment at temperatures >420 °C [36,42]. As a result, after heat treatment at 500 °C, the *I* phase (if present) in MgZn5.5Y2 is either transformed into the *W* phase or dissolved. Additionally, in accordance with existing literature, during high-temperature heat treatment (>500 °C), the polytype of the LPSO phase must change from 18R to 14H [43].

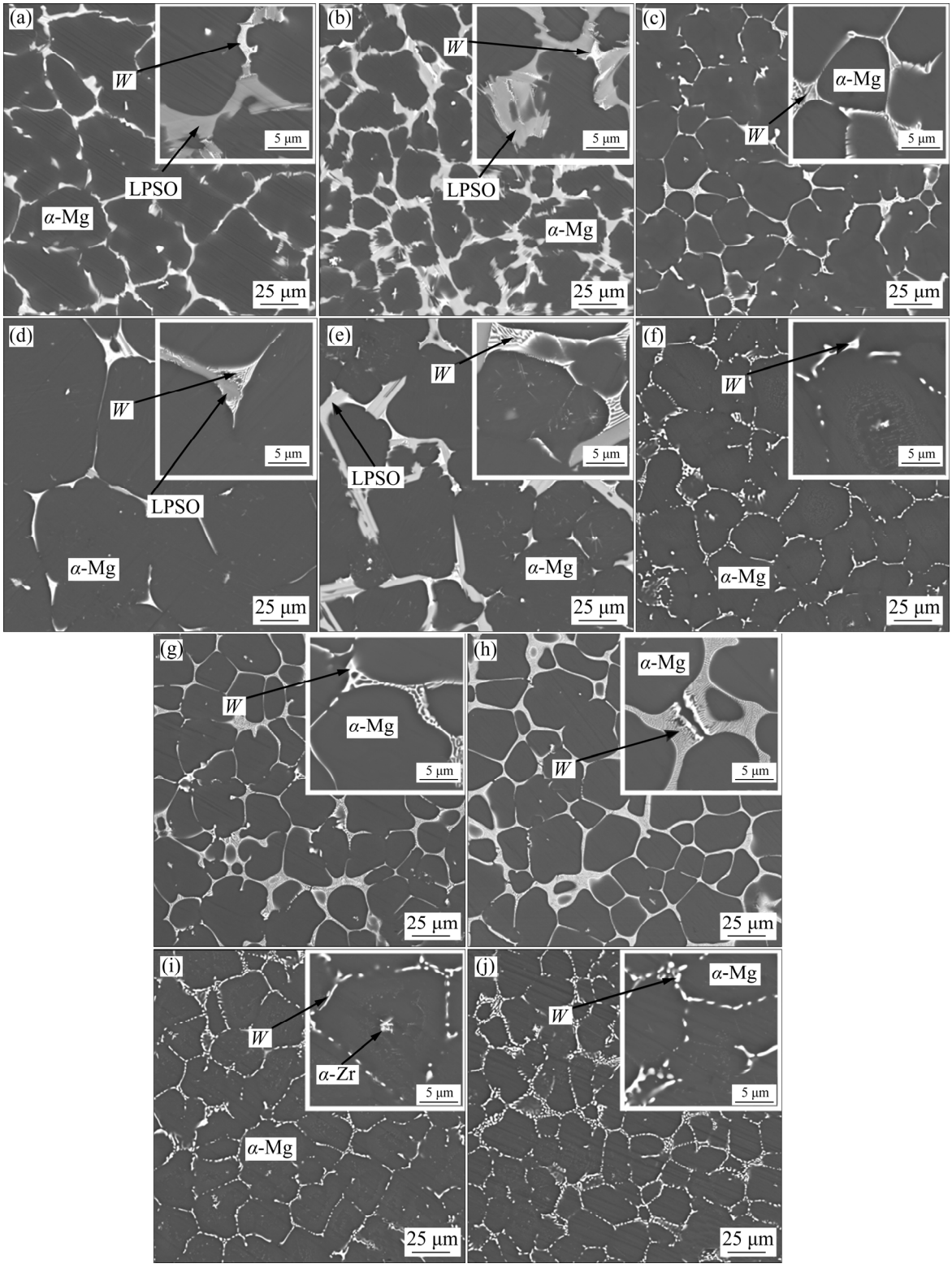

Fig. 4 Microstructures of Mg−Zn−Y−Zr alloys in as-cast condition (a, b, c, g, h) and after SSHT for 6 h at 540 °C (d, e) and 500 °C (f, i, j): (a, d) MgZn2.5Y3.5; (b, e) MgZn3.5Y5.5; (c, f) MgZn5.5Y2; (g, i) MgZn5.5Y3.5; (h, j) MgZn5.5Y4.5

Hereafter, for simplicity, only the main secondary phase has been indicated when the alloys are described. Accordingly, the MgZn2.5Y3.5 and MgZn3.5Y5.5 are alloys with LPSO phase and MgZn5.5Y2, MgZn5.5Y3.5 and MgZn5.5Y4.5 are alloys with *W* phase.

Table 2 Compositions of alloy phases in as-cast condition obtained by EDS (at.%)

Alloy	LPSO (light gray)				*W* (white)			
	Mg	Zn	Y	Zn/Y molar ratio	Mg	Zn	Y	Zn/Y molar ratio
MgZn2.5Y3.5	Bal.	4.2	5.6	0.75:1	Bal.	9.9	6.8	1.5:1
MgZn3.5Y5.5	Bal.	4.0	5.5	0.75:1	Bal.	11.1	7.3	1.5:1
MgZn5.5Y2	–	–	–	–	Bal.	12.7	6.9	1.8:1
MgZn5.5Y3.5	–	–	–	–	Bal.	12.4	7.5	1.7:1
MgZn5.5Y4.5	–	–	–	–	Bal.	13.4	8.7	1.5:1

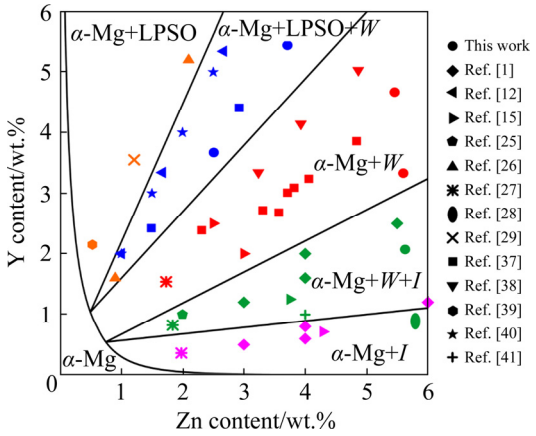

Fig. 5 Reconstructed solidus surface projection of Mg−Zn−Y system at Mg corner

3.3 Heat treatment regime

The Brinell hardness, electrical conductivity, content of eutectic phase, and grain sizes of the Mg−Zn−Y−Zr alloys during SSHT are shown in Fig. 6. The SSHT temperature was 540 °C for MgZn2.5Y3.5 and MgZn3.5Y5.5 alloys and 500 °C for MgZn5.5Y2, MgZn5.5Y3.5, and MgZn5.5Y4.5 alloys. These temperatures were chosen based on the Scheil−Gulliver solidification calculations and thermal analysis results [9,12,14]. The hardness of the MgZn2.5Y3.5 alloy after SSHT for 6 h is slightly increased, whereas the electrical conductivity is decreased. The volume fraction of the *W* phase remains constant, but the LPSO phase content is reduced from 10 vol.% in the as-cast condition to 1.4 vol.% after heat treatment for 6 h. Further increase in the time of heat treatment has no effect on the aforementioned parameters. The grain size of the MgZn2.5Y3.5 alloy increases during SSHT and the grain sizes are 34, 67, and 109 μm in the as-cast condition, after 6 h of heat treatment, and after 18 h of heat treatment, respectively. Different results are observed for the MgZn3.5Y5.5 alloy with the LPSO structure because SSHT does not impact the hardness and electrical conductivity. Interesting changes in the phase composition are observed for this alloy. After heat treatment for 18 h, the LPSO phase content decreases from 17.3 to 5.7 vol.%, but the *W* phase content increases from 1.2 to 3.7 vol.%. A possible explanation of this phenomena is non-equilibrium alloy solidification. At high cooling rates, the composition of the liquid phase during solidification can change significantly as compared to the equilibrium composition, leading to the solidification of different eutectics [44]. When heat treatment is carried out, the alloy phase composition becomes the equilibrium phase composition, which promotes the dissolution of the LPSO phase and the formation of the *W* phase. The grain size of the alloy increases with the duration of SSHT, but the increase is not as significant as that for the MgZn2.5Y3.5 alloy.

The hardness of MgZn5.5Y2, MgZn5.5Y3.5, and MgZn5.5Y4.5 alloys in which only the *α*-Mg+*W* eutectic is observed, decreases with increasing SSHT time. After SSHT for 6 h, an increase in the electrical conductivity is observed for the MgZn5.5Y2 and MgZn5.5Y3.5 alloys, but there was no change for the MgZn5.5Y4.5 alloy. The *W* phase content decreases in the MgZn5.5Y3.5 and MgZn5.5Y4.5 alloys but remains almost constant in MgZn5.5Y2 alloy. This result is unusual because the contents of Zn and Y in *α*-Mg should increase with the dissolution of the *W* phase. An increase in the content of the elements in *α*-Mg should lead to a decline in the electrical conductivity. The observed discrepancy can be accounted for the influence of the *W* phase content on the electrical conductivity of the alloy and the initial dendritic segregation in the as-cast condition. The results of the grain size measurements reveal that there is a maximum increase in the grain size

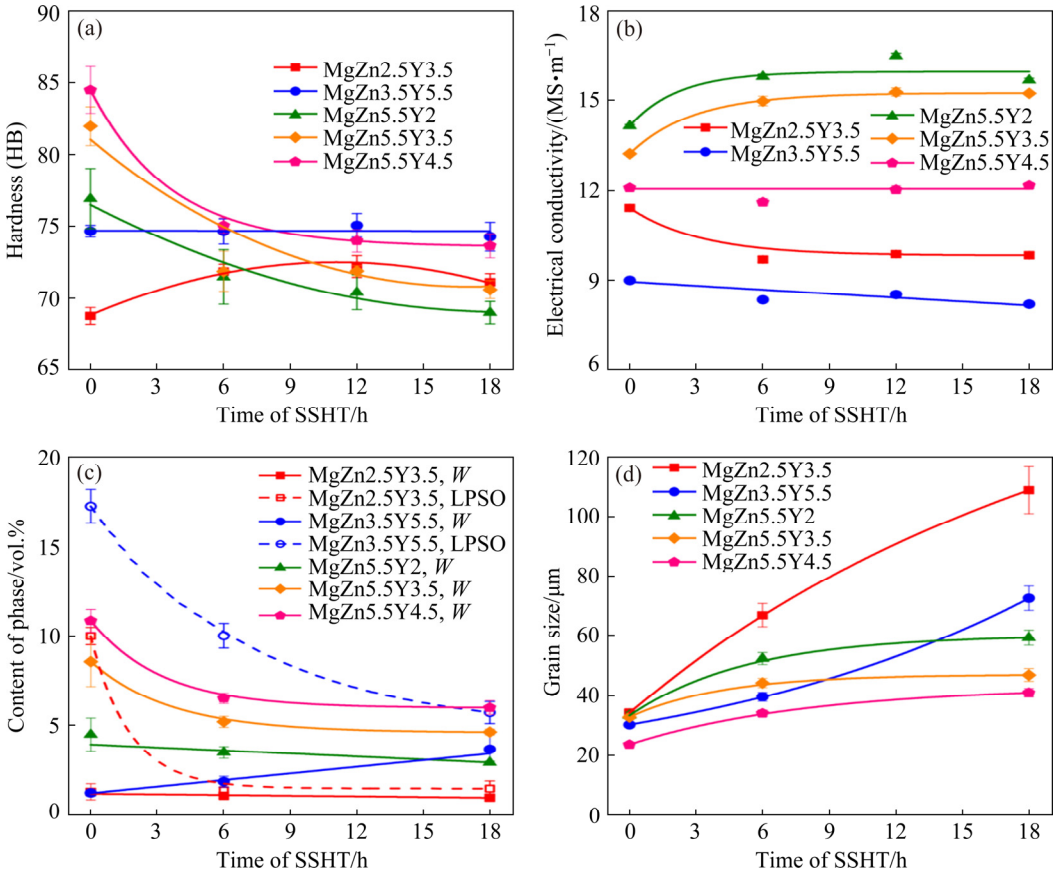

Fig. 6 Brinell hardness (a), electrical conductivity (b), content of phases (c), and grain size (d) of Mg−Zn−Y−Zr alloys during SSHT at 540 °C for MgZn2.5Y3.5 and MgZn3.5Y5.5 alloys and at 500 °C for MgZn5.5Y2, MgZn5.5Y3.5, and MgZn5.5Y4.5 alloys

after SSHT for 6 h and any further increase in the duration of SSHT beyond 6 h has a negligible effect on the grain sizes of the MgZn5.5Y2, MgZn5.5Y3.5, and MgZn5.5Y4.5 alloys. Therefore, SSHT for 6 h was adequate for all of the investigated alloys.

In order to determine the appropriate aging regime after SSHT at 540 °C (MgZn2.5Y3.5, and MgZn3.5Y5.5) and 500 °C (MgZn5.5Y2, MgZn5.5Y3.5, and MgZn5.5Y4.5), the alloys were aged at temperatures from 150 to 300 °C. During aging, the hardness and electrical conductivity of the alloy samples were measured every 4 h, as shown in Fig. 7. The maximum hardness for the MgZn2.5Y3.5 and MgZn3.5Y5.5 alloys was obtained when the alloy was aged at 150 °C. The hardness increased during the first 8 h due to precipitation hardening; subsequently, the hardness almost remained constant.

For the alloys with α-Mg+W eutectic structures, the maximum hardness is achieved at 200−250 °C after 4−8 h. The maximum increase in the electrical conductivity for both alloys with LPSO and W phases was observed during aging at 300 °C. The increase in the electrical conductivity was associated with the depletion of α-Mg during the aging process. When the aging temperature was 300 °C, overaging occurred. After aging at 300 °C, the lamellas of the LPSO phase were precipitated in the α-Mg. The LPSO lamellas were also observed in the MgZn4.9Y8.9 alloy heat treated at 400 °C for 10 h, where the mechanical properties decreased following heat treatment [23]. In accordance with the results obtained, aging at 150 °C for 8 h is recommended for alloys with the LPSO phase and aging at 200 °C for 8 h is recommended for alloys with W phase.

For all alloys, the increase in hardness during aging is very low, <10 HB, when compared to that of the SSHT condition. In this case, the expected increase in the strength of the alloys after T6 heat treatment cannot be very high. The low strengthening effect of the fcc W phase is related to the weak bonding with the hcp Mg matrix [5]. It has

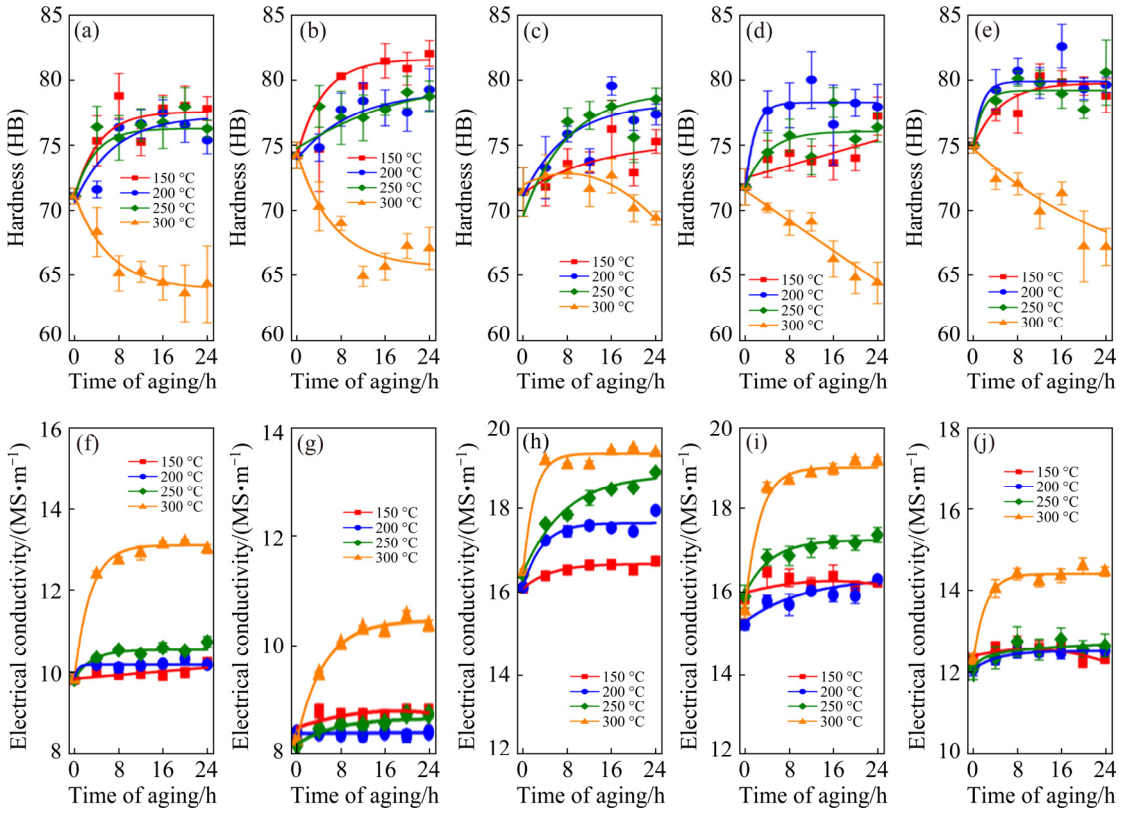

Fig. 7 Hardness (a−e) and electrical conductivity (f−j) of Mg−Zn−Y−Zr alloys during aging at different temperatures after SSHT: (a, f) MgZn2.5Y3.5; (b, g) MgZn3.5Y5.5; (c, h) MgZn5.5Y2; (d, i) MgZn5.5Y3.5 and (e, j) MgZn5.5Y4.5

been previously shown that the LPSO phase is more effective for strengthening Mg alloys; however, no significant effect was observed during heat treatment, based on the hardness measurement results. Further investigation to discover elements that can promote an increased strengthening response during aging is required.

3.4 Phase compositions

Figure 8 shows the XRD spectra of the MgZn3.5Y5.5 and MgZn5.5Y4.5 alloys in as-cast conditions after being subjected to SSHT and aging. The as-cast MgZn3.5Y5.5 alloy structure was observed to consist of α-Mg, LPSO, and *W* phases, thereby confirming the EDS results. The SSHT carried out at 540 °C for 6 h and the aging process performed at 150 °C for 8 h led to an increase in the relative intensity of diffraction peaks that corresponded to the *W* phase. However, no new phases were formed during heat treatment. In accordance with Ref. [25], the formation of *W*, $\beta1'$, and $\beta2'$ precipitates was possible in Mg−Zn−Y alloys. Furthermore, the α-Mg and *W* phases were found in the MgZn5.5Y4.5 alloy in the as-cast

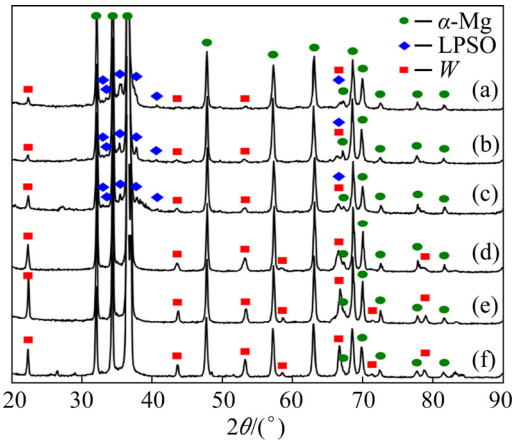

Fig. 8 XRD patterns of MgZn3.5Y5.5 (a−c) and MgZn5.5Y4.5 (d−f) alloys: (a, d) As-cast; (b, e) After 6 h of SSHT; (c, f) After 6 h of SSHT + 8 h of aging

condition, which confirmed the EDS analysis results; no significant changes could be observed after the alloy was subjected to 6 h of SSHT at 500 °C and 8 h of aging at 200 °C.

3.5 Fluidity and hot tearing susceptibility

Figure 9 shows the fluidity of the Mg−Zn−Y−Zr alloys. The fluidity probe lengths for the

Mg−Zn−Y−Zr alloys were in the 364−415 mm range for all of the alloys. The maximum probe length of 415 mm was achieved for the MgZn5.5Y4.5 alloy and the lowest fluidity was observed for the MgZn2.5Y3.5 alloy. This suggests that alloys with the *W* phase have a higher fluidity, even though the difference between the fluidity of alloys with the *W* and LPSO phases is minor. The fluidity of the commonly available AZ91 magnesium commercial alloy was 410 mm [37], which is close to the results obtained for the Mg−Zn−Y−Zr alloys.

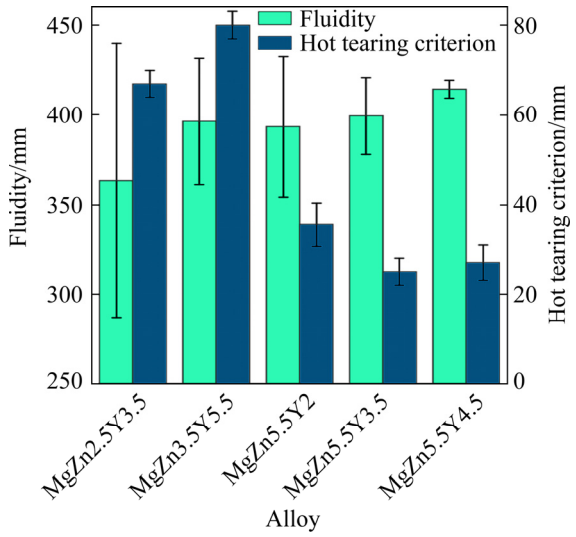

Fig. 9 Fluidity and hot tearing criterion of Mg−Zn−Y−Zr alloys

The hot tearing criterion (the maximum length of dog-bone section without cracks) for the Mg−Zn−Y−Zr alloys is presented in Fig. 9. The hot tearing criterion for the MgZn2.5Y3.5 and MgZn3.5Y5.5 alloys with LPSO phases was 67 and 80 mm, respectively. Figure 1 shows the dog-bone probe used; and, as can be seen, the maximum length of the dog-bone section is 80 mm. The hot tearing criterion for alloys with the *W* phase, i.e., MgZn5.5Y2, MgZn5.5Y3.5, and MgZn5.5Y4.5 was 35, 25 and 27 mm, respectively. The AZ91 alloy hot tearing criterion obtained on the same hot tearing test was 50−56 mm [37,45], which means that alloys with the LPSO phase exhibit higher resistance to hot tearing formation during casting than alloys with *W* phases and then AZ91 alloys. The hot tearing susceptibility is dependent on the grain size of the alloy [46]; and, in accordance with our results (Fig. 6(d)), the grain size in the as-cast condition is almost the same for investigated alloys. The probable reason for the lower hot tearing susceptibility of alloys with LPSO phases is the higher volume of eutectics that increase the refilling ability during the later stage of solidification. Also, alloys with LPSO phases exhibit less freezing ranges than those with *W* phases. WEI et al [12] demonstrate that the solid fraction at the coherency point is higher and the number of hot tearing nucleation decreases in alloys with LPSO phase when compared to alloys with *W* phase.

3.6 Mechanical properties

The mechanical properties of the Mg−Zn−Y−Zr alloys after T6 heat treatment are shown in Fig. 10. Based on the results obtained in Section 3.5 for the MgZn2.5Y3.5 and MgZn3.5Y5.5 alloys with LPSO phases, SSHT (540 °C, 6 h) followed by water quenching and aging (150 °C, 8 h) was performed. The heat treatment regime involving SSHT (500 °C, 6 h) followed by water quenching and aging (200 °C, 8 h) was used for alloys with *W* phases (MgZn5.5Y2, MgZn5.5Y3.5, and MgZn5.5Y4.5). The YS of alloys with LPSO phases was ~150 MPa. However, for the alloys with *W* phases, the YS was 120, 127, and 136 MPa for MgZn5.5Y2, MgZn5.5Y3.5, and MgZn5.5Y4.5, respectively. Figure 11 depicts the YS of Mg−Zn−Y−Zr alloys vs the composition of α-Mg

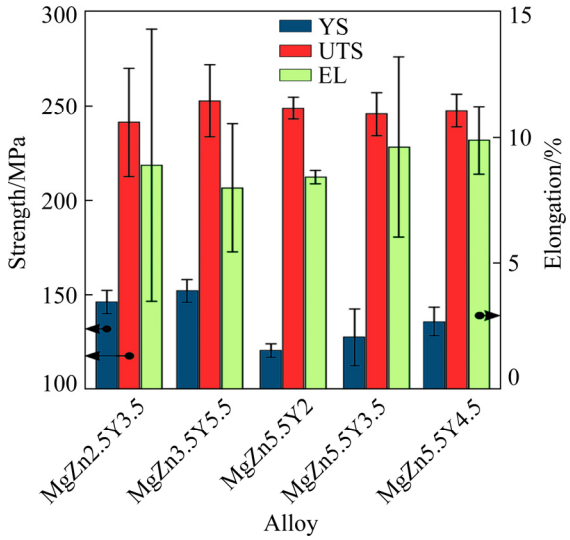

Fig. 10 Mechanical properties of Mg−Zn−Y−Zr alloys after T6 heat treatment: SSHT (540 °C, 6 h) followed by water quenching and aging (150 °C, 8 h) for MgZn2.5Y3.5 and MgZn3.5Y5.5 alloys; SSHT (500 °C, 6 h) followed by water quenching and aging (200 °C, 8 h) for MgZn5.5Y2, MgZn5.5Y3.5, and MgZn5.5Y4.5 alloys

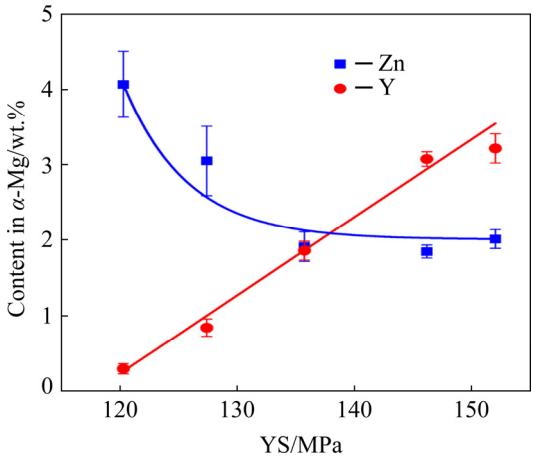

Fig. 11 YS of Mg−Zn−Y−Zr alloys after T6 heat treatment vs composition of α-Mg

obtained from EDS analysis after SSHT for 6 h. In α-Mg, the YS increases as the Y content increases and the Zn content decreases. The UTS and EL are similar for all alloys (~250 MPa and ~9%, respectively). The mechanical properties of the specimens are higher, particularly EL, when compared with the properties of the Mg−Zn−Y alloys in the as-cast condition [11,26,38,40].

3.7 Corrosion resistance

Figure 12 illustrates the polarization curves of Mg−Zn−Y−Zr alloys after T6 heat treatment in 3 wt.% NaCl aqueous solution. The corrosion current density, corrosion potential, and corrosion rate of alloys have been determined using Tafel fitting and are shown in Table 3. The corrosion potentials of the MgZn2.5Y3.5 and MgZn3.5Y5.5 alloys were (−1.58±0.01) and (−1.55±0.01) V (vs Ag/AgCl), respectively. These values are in agreement with those previously reported [4,26,29], and more noble corrosion potentials are observed with the increasing amount of the LPSO phase, which acts as a cathode to α-Mg. The increased amount of the LPSO phase leads to minor increase in both anodic and cathodic current densities (Fig. 12(a)), which is in agreement with Refs. [4,26].

Similar corrosion potentials (approximately (−1.52±0.01) V (vs Ag/AgCl)) were obtained for the MgZn5.5Y2, MgZn5.5Y3.5, and MgZn5.5Y4.5 alloys with *W* phase in structure. Thus, we can conclude that alloys with *W* phases exhibit more noble corrosion potentials than alloys with LPSO phases, but the difference is not large. The anodic current density is almost identical for alloys with *W* phase, but the cathodic current density increases as the Y content and amount of the *W* phase in the alloy increase. The cathodic reaction became easier kinetically as the amount of the *W* phase in the alloy increased, which in turn promoted a higher corrosion rate.

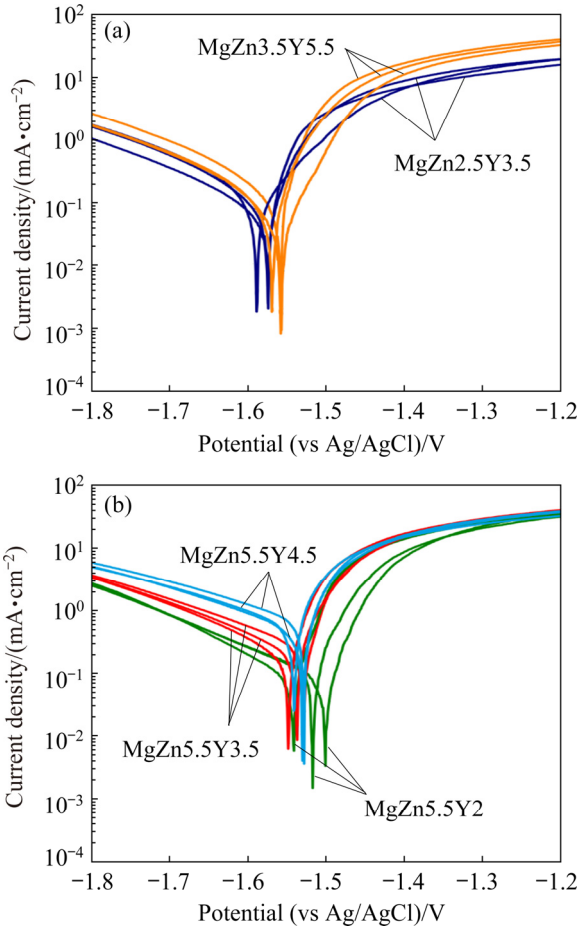

Fig. 12 Polarization curves of T6 heat-treated Mg−Zn−Y−Zr alloys in 3 wt.% NaCl aqueous solution: (a) Alloys with LPSO phases; (b) Alloys with *W* phases

A similar result was obtained by CHEN et al [47] when comparing the corrosion rates of MgZn6Y1 (ZW61) and MgZn10Y1 (ZW101) alloys; the formation of the Mg_7Zn_3 phase in the ZW101 alloy, which like the *W* phase is a cathodic structural component, leads to a significant increase in the corrosion rate as compared to that of the ZW61 alloy without Mg_7Zn_3. In Ref. [47], a small deviation in the corrosion potentials of ZW61 and ZW101 alloys was also obtained, namely, 1.519 and −1.509 V, respectively. The shift of the corrosion potential toward the positive side is explained by an increase in the concentration of Zn in the alloy,

Table 3 Electrochemical and immersion corrosion test data obtained for Mg−Zn−Y−Zr alloys subjected to T6 heat treatment in 3 wt.% NaCl aqueous solution

Alloy	Electrochemical corrosion test			Immersion corrosion test
	φ_{corr}(vs Ag/AgCl)/V	J_{corr}/(μA·cm^{-2})	Corrosion rate/(mm·year^{-1})	Corrosion rate/(mm·year^{-1})
MgZn2.5Y3.5	−1.58±0.01	102.8±15.2	2.34±0.34	2.50±0.43
MgZn3.5Y5.5	−1.55±0.01	116.3±45.2	2.64±1.02	5.29±1.52
MgZn5.5Y2	−1.52±0.02	93.3±6.5	2.11±0.15	6.59±0.92
MgZn5.5Y3.5	−1.53±0.01	258.8±36.6	5.86±0.83	11.61±0.47
MgZn5.5Y4.5	−1.52±0.01	541.1±115.1	12.24±2.60	136.37±8.16

which is more positive with respect to magnesium. Furthermore, the increase in the corrosion rate is supported by the disinhibition of a similar electrochemical process.

The effect of the LPSO phase on the corrosion properties is ambiguous. On one hand, the LPSO phase, like the *W* phase, is a cathodic structural component and should contribute to the increase in the corrosion rate; however, the corrosion rate of alloys with the LPSO phase is lower than that of the alloys with the *W* phase. WANG et al [48] have recently reported that LPSO phases enhance corrosion by acting as cathodic phases, thereby accelerating microgalvanic corrosion. However, alloys with low quantity of LPSO phase show better corrosion resistance than those with more noble precipitates. Unfortunately, the mechanism of the combined effect of the *W* and LPSO phases on the corrosion resistance of magnesium alloys remains unclear and requires further research. It is highly probable that alloys with the LPSO phase can quickly regenerate the oxide film present on the corrosion products, which effectively inhibits the contact between the solution and the metal.

The corrosion rates of the Mg–Zn–Y–Zr alloys obtained using electrochemical and immersion corrosion tests are shown in Fig. 13. The low corrosion rate of ~2.2 mm/year was observed for the MgZn2.5Y3.5, MgZn3.5Y5.5, and MgZn5.5Y2 alloys with accordance to the results of the polarization test. The corrosion rate for alloys with a larger quantity of the *W* phase was obtained using Tafel plots and observed to be higher. The corrosion rates for the MgZn5.5Y3.5 and MgZn5.5Y4.5 alloys were ~5.9 and ~12.2 mm/year, respectively. The electrochemical corrosion test is an express test that only represents a snapshot of corrosion at the time it is performed [49]. Hence, immersion tests are more appropriate for obtaining the long-term

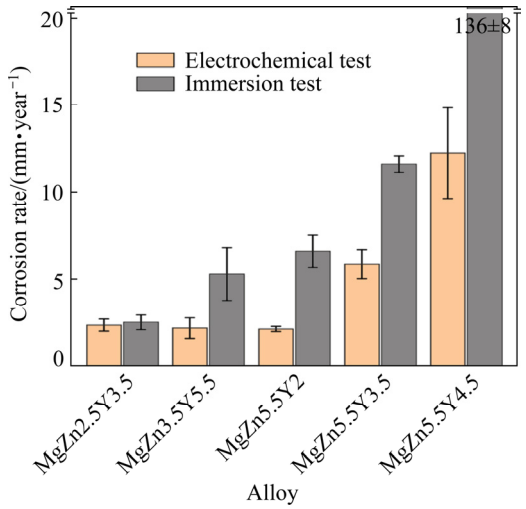

Fig. 13 Corrosion rates of T6 heat treated Mg–Zn–Y–Zr alloys obtained by electrochemical and immersion corrosion testing in 3 wt.% NaCl aqueous solution

corrosion rates of Mg alloys. The corrosion rate of the MgZn2.5Y3.5 alloy obtained via the immersion test (~2.5 mm/year) is the same as that obtained by the polarization test (~2.2 mm/year). The long-term corrosion test revealed that the higher LPSO phase content in the MgZn3.5Y5.5 alloy increased the corrosion rate to ~5.3 mm/year. The corrosion rates of MgZn5.5Y2, MgZn5.5Y3.5, and MgZn5.5Y4.5 alloys with *W* phases were ~6.6, ~11.6, and ~136.4 mm/year, respectively. Consequently, the increased *W* phase content significantly increased the corrosion rates of the alloys. A similar effect was obtained by the CHEN et al [47], wherein an increase in the content and area of cathodic structural components in the ZW101 alloy significantly increased its corrosion rate.

4 Conclusions

(1) Alloys with LPSO, *W*, and *I* eutectic phases can be obtained, in accordance with the Thermo-Calc calculation results in the Mg−

(0−6)wt.%Zn−(0−6)wt.%Y composition range. The calculation of alloy solidification pathways shows that alloys with LPSO phase have a less freezing range than alloys with *W* phase.

(2) The T6 heat treatment regime consisting of SSHT at 540 °C for 6 h followed by water quenching and aging at 150 °C for 8 h is recommended for alloys with LPSO phases. However, the SSHT at 500 °C for 6 h followed by water quenching and aging at 200 °C for 8 h can be recommended for alloys with *W* phases.

(3) The alloys with LPSO phase have lower hot tearing susceptibilities than alloys with *W* phase and the widespread commercial AZ91 alloy, which confirm the short freezing range of alloys with LPSO phase. The fluidity of alloys with LPSO and *W* phases is the same as that for the AZ91 alloy.

(4) The UTS and EL (~250 MPa and ~9%, respectively) of the investigated Mg−Zn−Y−Zr alloys are almost identical. The YS is 150 and 120−136 MPa for the alloys with LPSO and *W* phases, respectively. The YS of alloys is related to the composition of α-Mg.

(5) The corrosion rate of the alloys with LPSO phases in 3 wt.% NaCl aqueous solution obtained using immersion and polarization tests was lower than that of the alloys with *W* phases. The lowest corrosion rate (2 mm/year) was observed for Mg−2.5Zn−3.7Y− 0.3Zr alloy.

(6) In summary, it can be concluded that Mg−Zn−Y−Zr alloys with LPSO phases are the most favorable candidates for using as casting alloys due to their superior casting, corrosion, and mechanical properties. Hence, these alloys should be considered for further investigation to discover elements that can promote an increased strengthening response during heat treatment.

Acknowledgments

The authors gratefully acknowledge the financial support of the Ministry of Science and Higher Education of the Russian Federation in the framework of Increase Competitiveness Program of NUST «MISiS» (No. К2-2020-025), implemented by a governmental decree dated 16th of March 2013, N 211.

References

[1] LEE J Y, KIM D H, LIM H K, KIM D H. Effects of Zn/Y ratio on microstructure and mechanical properties of Mg−Zn−Y alloys [J]. Materials Letters, 2005, 59: 3801−3805. https://doi.org/10.1016/j.matlet.2005.06.052.

[2] OKAYASU M, TAKEUCHI S, MATSUSHITA M, TADA N, YAMASAKI M, KAWAMURA Y. Mechanical properties and failure characteristics of cast and extruded Mg97Y2Zn1 alloys with LPSO phase [J]. Materials Science and Engineering A, 2016, 652: 14−29. https://doi.org/10.1016/j.msea.2015.11.069.

[3] SINGH A, OSAWA Y, SOMEKAWA H, MUKAI T. Ultra-fine grain size and isotropic very high strength by direct extrusion of chill-cast Mg−Zn−Y alloys containing quasicrystal phase [J]. Scripta Materialia, 2011, 64: 661−664. https://doi.org/10.1016/j.scriptamat.2010.12.016.

[4] ZHANG Z Q, LIU X, HU W Y, LI J H, LE Q C, BAO L, ZHU Z J, CUI J Z. Microstructures, mechanical properties and corrosion behaviors of Mg−Y−Zn−Zr alloys with specific Y/Zn mole ratios [J]. Journal of Alloys and Compounds, 2015, 624: 116−125. https://doi.org/10.1016/j.jallcom.2014.10.177.

[5] TAHREEN N, CHEN D L. A critical review of Mg−Zn−Y series alloys containing *I*, *W*, and LPSO phases: A critical review of Mg−Zn−Y series alloys containing *I*, *W*, and LPSO phases [J]. Advanced Engineering Materials, 2016, 18: 1983−2002. https://doi.org/10.1002/adem.201600393.

[6] XU D K, TANG W N, LIU L, XU Y B, HAN E H. Effect of *W*-phase on the mechanical properties of as-cast Mg−Zn−Y−Zr alloys [J]. Journal of Alloys and Compounds, 2008, 461: 248−252. https://doi.org/10.1016/j.jallcom.2007.07.096.

[7] LUO Z P, ZHANG S Q. High-resolution electron microscopy on the X−Mg12ZnY phase in a high strength Mg−Zn−Zr−Y magnesium alloy [J]. Journal of Materials Science Letters, 2000, 19: 813–815. https://doi.org/10.1023/A:1006793411506.

[8] XU D K, LIU L, XU Y B, HAN E H. The fatigue behavior of *I*-phase containing as-cast Mg−Zn−Y−Zr alloy [J]. Acta Materialia, 2008, 56: 985−994. https://doi.org/10.1016/j.actamat.2007.10.057.

[9] BAE D H, KIM S H, KIM D H, KIM W T. Deformation behavior of Mg−Zn−Y alloys reinforced by icosahedral quasicrystalline particles [J]. Acta Materialia, 2002, 50: 2343−2356. https://doi.org/10.1016/S1359-6454(02) 00067-8.

[10] KAWAMURA Y, HAYASHI K, INOUE A, MASUMOTO T. Rapidly solidified powder metallurgy $Mg_{97}Zn_1Y_2$ alloys with excellent tensile yield strength above 600 MPa [J]. Materials Transactions, 2001, 42: 1172−1176.

[11] XU D K, TANG W N, LIU L, XU Y B, HAN E H. Effect of Y concentration on the microstructure and mechanical properties of as-cast Mg–Zn–Y–Zr alloys [J]. Journal of Alloys and Compounds, 2007, 432: 129–134. https://doi.org/10.1016/j.jallcom.2006.05.123

[12] WEI Z, WANG Y, LIU Z. Effects of Zn and Y on hot-tearing susceptibility of Mg–*x*Zn–2*x*Y alloys [J]. Materials Science and Technology, 2018, 34: 2001–2007. https://doi.org/10.1080/02670836.2018.1507696.

[13] WANG Z, HUANG Y D, SRINIVASAN A, LIU Z, KAINER K U, HORT N. Influences of y additions on the hot tearing

susceptibility of Mg−1.5wt%Zn alloys [J]. Materials Science Forum, 2013, 765: 306−310. https://doi.org/10.4028/www.scientific.net/MSF.765.306.

[14] WEI Z Q, LIU Z, SHENG X F, WANG Y, ZHANG Z L, JU Y D. Effects of Y and Zn/Y on hot tearing susceptibility of Mg−Zn−Y−Zr alloys [J]. Materials Science and Technology, 2019, 35: 1872–1882. https://doi.org/10.1080/02670836.2019.1652405.

[15] JIA D R, LIU Z, MAO P L, WANG F, WANG Z. Hot tearing behavior of Mg–5(Zn+Y)−0.5Zr alloys [J]. Materials Research Express, 2017, 4: 106511. https://doi.org/10.1088/2053-1591/aa90a2.

[16] GENG J W, TENG X X, ZHOU G R, ZHAO Z W. Solidification and microstructure of as-cast Mg65Zn32Y3 quasicrystal alloy [J]. Physica B: Condensed Matter, 2013, 420: 64−69. https:// doi.org/10.1016/j.physb.2013.03.035.

[17] TAN Q, ATRENS A, MO N, ZHANG M X. Oxidation of magnesium alloys at elevated temperatures in air: A review [J]. Corrosion Science, 2016, 112: 734−759. https://doi.org/10. 1016/j.corsci.2016.06.018.

[18] WANG J F, LU R P, WEI W W, HUANG X F, PAN F S. Effect of long period stacking ordered (LPSO) structure on the damping capacities of Mg–Cu–Mn–Zn–Y alloys [J]. Journal of Alloys and Compounds, 2012, 537: 1–5. https://doi.org/10.1016/ j.jallcom.2012.05.003.

[19] WANG J, ZHANG J S, ZONG X M, XU C X, YOU Z Y, NIE K B. Effects of Ca on the formation of LPSO phase and mechanical properties of Mg−Zn−Y−Mn alloy [J]. Materials Science and Engineering A, 2015, 648: 37−40. https://doi.org/10.1016/j.msea.2015.09.046.

[20] WU J, CHIU Y L, JONES I P. Microstructure of as-cast Mg−4.2Zn−0.8Y (at.%) alloys containing Gd [J]. Journal of Physics: Conference Series, 2014, 522: 012033. https://doi.org/10.1088/1742-6596/522/1/012033.

[21] YANG K, ZHANG J S, ZONG X M, WANG W X, XU C X, CHENG W L, NIE K B. Effect of microalloying with boron on the microstructure and mechanical properties of Mg−Zn−Y−Mn alloy [J]. Materials Science and Engineering A, 2016, 669: 340−343. https://doi.org/10.1016/j.msea.2016.05.095.

[22] STJOHN D H, QIAN M A, EASTON M A, CAO P, HILDEBRAND Z. Grain refinement of magnesium alloys [J]. Metallurgical and Materials Transactions A, 2005, 36: 1669–1679. https://doi.org/10.1007/s11661-005-0030-6.

[23] LU R P, WANG J F, CHEN Y L, QIN D Z, YANG W X, WU Z S. Effects of heat treatment on the morphology of long-period stacking ordered phase, the corresponding damping capacities and mechanical properties of Mg–Zn–Y alloys [J]. Journal of Alloys and Compounds, 2015, 639: 541–546. https://doi.org/ 10.1016/j.jallcom.2015.03.208.

[24] MA R, DONG X P, YAN B S, CHEN S Q, LI Z B, PAN Z, LING H J, FAN Z T. Mechanical and damping properties of thermal treated Mg–Zn–Y–Zr alloys reinforced with quasicrystal phase [J]. Materials Science and Engineering A, 2014, 602: 11–18. https://doi.org/10.1016/j.msea.2014.02.055.

[25] YAN B S, DONG X P, MA R, CHEN S Q, PAN Z, LING H J. Effects of heat treatment on microstructure, mechanical properties and damping capacity of Mg–Zn–Y–Zr alloy [J]. Materials Science and Engineering A, 2014, 594: 168–177. https://doi.org/10.1016/j.msea.2013.11.019.

[26] LI C Q, XU D K, ZENG Z R, WANG B J, SHENG L Y, CHEN X B, HAN E H. Effect of volume fraction of LPSO phases on corrosion and mechanical properties of Mg−Zn−Y alloys [J]. Materials & Design, 2017, 121: 430–441. https://doi.org/10.1016/j.matdes.2017.02.078.

[27] ZHANG E L, HE W W, DU H, YANG K. Microstructure, mechanical properties and corrosion properties of Mg–Zn–Y alloys with low Zn content [J]. Materials Science and Engineering A, 2008, 488: 102−111. https://doi.org/10.1016/j.msea.2007.10.056.

[28] SONG Y W, SHAN D Y, CHEN R S, HAN E H. Effect of second phases on the corrosion behaviour of wrought Mg−Zn−Y−Zr alloy [J]. Corrosion Science, 2010, 52: 1830−1837. https:// doi.org/10.1016/j.corsci.2010.02.017.

[29] ZHANG J, XU J, CHENG W, CHEN C, KANG J. Corrosion behavior of Mg–Zn–Y alloy with long-period stacking ordered structures [J]. Journal of Materials Science & Technology, 2012, 28: 1157–1162. https://doi.org/10.1016/S1005-0302(12)60186-8.

[30] ANDERSSON J O, HELANDER T, HÖGLUND L, SHI P F, SUNDMAN B. Thermo-Calc & DICTRA, computational tools for materials science [J]. CALPHAD, 2002, 26: 273–312. https://doi.org/10.1016/S0364-5916(02)00037-8.

[31] Thermo-Calc software TCMG4 magnesium alloys database (Version 4) [Z]. 2019.

[32] ASTM standard G102—89. Standard practice for calculation of corrosion rates and related information from electrochemical measurements [S]. West Conshohocken, ASTM International, 2015. https://doi.org/10.1520/G0102-89R15E01.

[33] ASTM standard G1—03. Standard practice for preparing, cleaning, and evaluating corrosion test specimens [S]. West Conshohocken: ASTM International, 2011. https://doi.org/10.1520/G0001-03R17E01.

[34] RAVI K R, PILLAI R M, AMARANATHAN K R, PAI B C, CHAKRABORTY M. Fluidity of alloys and composites: A review [J]. Journal of Alloys and Compounds, 2008, 456: 201–210. https://doi.org/10.1016/j.jallcom.2007.02.038.

[35] SCHEIL E. Comments on the crystal layers formation [J]. Journal of Metallurgy, 1942, 34: 70–72.

[36] GENG J W, TENG X Y, ZHOU G G, ZHAO D G. Microstructure transformations in the heat-treated Mg–Zn–Y alloy [J]. Journal of Alloys and Compounds, 2013, 577: 498–506. https://doi.org/10.1016/j.jallcom.2013.07.009.

[37] BAZHENOV V E, KOLTYGIN A V, SUNG M C, PARK S H, TSELOVALNIK YU V, STEPASHKIN A A, RIZHSKY A A, BELOV M V, BELOV V D, MALYUTIN K V Development of Mg−Zn−Y−Zr casting magnesium alloy with high thermal conductivity [J]. Journal of Magnesium and Alloys, 2021. https://doi.org/10.1016/j.jma.2020.11.20.

[38] XU D K, TANG W N, LIU L, XU Y B, HAN E H. Effect of *W*-phase on the mechanical properties of as-cast Mg–Zn–Y–Zr alloys [J]. Journal of Alloys and Compounds, 2008, 461: 248–252. https://doi.org/10.1016/j.jallcom.2007.07.096.

[39] SHIRAISHI K, MAYAMA T, YAMASAKI M, KAWAMURA Y. Strain-hardening behavior and

microstructure development in polycrystalline as-cast Mg−Zn−Y alloys with LPSO phase subjected to cyclic loading [J]. Materials Science and Engineering A, 2016, 672: 49–58. https://doi.org/10.1016/j.msea.2016.06.069.

[40] TANG Y X, LI B, TANG H X, XU Y C, GAO Y P, WANG L H, GUAN J Y. Effect of long period stacking ordered structure on mechanical and damping properties of as-cast Mg–Zn–Y–Zr alloy [J]. Materials Science and Engineering A, 2015, 640: 287–294. https://doi.org/10.1016/j.msea.2015.06.004.

[41] YANG Y, ZHANG K, LI X G, LI Y J, MA M L, SHI G L, YUAN J W. Microstructure and phase transformation of as-cast and annealed Mg–4Zn–1Y alloy containing quasi-crystal phase [J]. Rare Metals, 2015, 34: 239–244. https://doi.org/10.1007/s12598-014-0443-8.

[42] LIU J F, YANG Z Q, YE H Q. In situ transmission electron microscopy investigation of quasicrystal-crystal transformations in Mg–Zn–Y alloys [J]. Journal of Alloys and Compounds, 2015, 621: 179–188. https://doi.org/10.1016/j.jallcom.2014.09.177.

[43] ITOI T, SEIMIYA T, KAWAMURA Y, HIROHASHI M. Long period stacking structures observed in Mg97Zn1Y2 alloy [J]. Scripta Materialia, 2004, 51: 107–111. https://doi.org/10.1016/j.scriptamat.2004.04.003.

[44] JIE W Q, ZHANG R J, ZHI H. Thermodynamic description of multi-component multi-phase alloys and its application to the solidification process [J]. Materials Science and Engineering A, 2005, 413–414: 497–503. https://doi.org/10.1016/j.msea. 2005.09.015.

[45] BAZHENOV V E, KOLTYGIN A V, SUNG M C, PARK S H, TITOV A YU, BAUTIN V A, MATVEEV S V, BELOV M V, BELOV V D, MALYUTIN K V. Design of Mg−Zn−Si−Ca casting magnesium alloy with high thermal conductivity [J]. Journal of Magnesium and Alloys, 2020, 8: 184–191. https://doi.org/10.1016/j.jma.2019.11.008.

[46] YANG Z Z, WANG K, FU P H, PENG L M, HU B, LIU M, SACHDEV A K. Influence of alloying elements on hot tearing susceptibility of Mg–Zn alloys based on thermodynamic calculation and experimental [J]. Journal of Magnesium and Alloys, 2018, 6: 44–51. https://doi.org/10.1016/j.jma.2018.01.001.

[47] CHEN X R, NING S C, WANG A, LE Q C, LIAO Q Y, JIA Y H, CHENG C L, LI X Q, ATRENS A, YU F X. Microstructure, mechanical properties and corrosion behavior of quasicrystal-reinforced Mg−Zn−Y alloy subjected to dual-frequency ultrasonic field [J]. Corrosion Science, 2020, 163: 108289. https://doi.org/10.1016/j.corsci.2019.108289.

[48] WANG Y J, ZHANG Y, WANG P P, ZHANG D, YU B W, XU Z, JIANG H T. Effect of LPSO phases and aged-precipitations on corrosion behavior of as-forged Mg–6Gd–2Y–1Zn–0.3Zr alloy [J]. Journal of Materials Research and Technology, 2020, 9: 7087–7099. https://doi.org/10.1016/j.jmrt.2020. 05.048.

[49] KIRKLAND N T, BIRBILIS N, STAIGER M P. Assessing the corrosion of biodegradable magnesium implants: A critical review of current methodologies and their limitations [J]. Acta Biomaterialia, 2012, 8: 925–936. https://doi.org/10.1016/j.actbio.2011.11.014.

含 LPSO 相和 *W* 相 Mg−Zn−Y−Zr 合金铸造、力学和腐蚀性能的比较

V. E. BAZHENOV, S. S. SAIDOV, Yu. V. TSELOVALNIK, O. O. VOROPAEVA, I. V. PLISETSKAYA, A. A. TOKAR, A. I. BAZLOV, V. A. BAUTIN, A. A. KOMISSAROV, A. V. KOLTYGIN, V. D. BELOV

National University of Science and Technology (MISiS), Leninskiy pr. 4, Moscow, 119049, Russia

摘　要：为了开发新型铸造镁合金，研究含长周期堆垛相(LPSO)和 *W* 共晶相的 Mg−Zn−Y−Zr 合金。硬度和电导率测试结果表明，T6 热处理的温度是合适的。与含 *W* 相的合金相比，含 LPSO 相合金的热裂敏感性更低，这与合金的凝固区间有关。然而，两者具有相同的流动性。在 T6 条件下，增加 Y 含量可以提高合金的屈服强度，但合金的其他拉伸性能基本相同。与含 *W* 相的合金相比，含 LPSO 相的合金具有更优的耐腐蚀性。含 LPSO 相的 Mg−2.5Zn−3.7Y−0.3Zr(质量分数，%)合金具有良好的铸造性能和力学性能，其腐蚀速率为 2 mm/year。

关键词：镁合金；铸造；LPSO 相；*W* 相；流动性；热裂敏感性；腐蚀速率

(Edited by Wei-ping CHEN)